

Lithologic and mineral information extraction for bauxite deposits exploration using ASTER data in the Wuchuan-Zheng'an-Daozhen area, northern Guizhou province, China

More than 20 laterite bauxite deposits have been discovered in the Wuchuan-Zheng'an-Daozhen region, northern Guizhou province, which is important bauxite orefield of China. Based on the reflectance spectra characteristics and low SiO₂ content of bauxite ore, this paper applied the Advanced Spaceborne Thermal Emission and Reflection Radiometer (ASTER) imagery to produce large-middle scale remote sensing geological interpretation, map the ore-bearing stratum, extract metallogenic zones for bauxite deposits by using Principal Component Analysis (PCA) and SiO₂ index. These results provide clues for future investigation of bauxite resources in this study area and an effective case reference for the remote sensing geological survey of bauxite.

Keywords: Guizhou, Wuchuan-Zheng'an-Daozhen area, bauxite, ASTER, PCA, SiO₂ content.

Introduction

As the rapid remote sensing technique development in spatial and spectral resolutions, remote sensing data have been widely used for geological mapping and mineral exploration in decades, and this is considered as one of the most significant applications in those areas[1-3]. As early in the 70s of last century, the Landsat multispectral images (MSS), SPOT images and radar images were used in geological mapping work for exploring lateritic bauxite[4]. At the end of 1980s, Chen Singling used remote sensing technology for trihydrate bauxite research in Guangxi province[5], which is the first remote sensing geological application of bauxite in China. P. Suman Babu used Landsat ETM+ to explore bauxite ore deposits by mixed tune matched filtering method in Panchpatmali, India[6]. Zhang Wenlong applied the SPOT5 data to survey of a bauxite deposit in the Kalimantan area of Indonesia[7]. The Advanced Spaceborne Thermal Emission and Reflection Radiometer (ASTER) was launched in 1999 and considered as an ideal tool for mineral exploration as the low-cost, large coverage area, and availability of ASTER data[8-9]. Zhang Yunfeng applied ASTER data to bauxite deposit pre-survey of Mianchi area in

northern China[10]. Cheng Gong applied ETM+ and ASTER remote sensing data to prospect lateritic bauxite in Laos[11].

Bauxite is the important economic Al resources and abundant in China, ranking fifth in the world. Huge number of bauxite ores have been identified in the Central Guizhou-southern Chongqing area in recent years. As a result of decades research and exploration carried out in the Wuchuan-Zheng'an-Daozhen (WZD) region, more than 20 lateritic bauxite deposits with more than 0.1 billion tonnes bauxite ores have been discovered (Fig.1.c). In addition, several other unexplored districts also show bauxite mineralization potential. Guo Jiao applied the Landsat8 OLI data for geological survey of bauxite deposits in Dazhuyuan-longxing area[12]. However, the application of remote sensing in the whole region is not carried out. This paper uses the ASTER image data for remote sensing lithologic tectonic interpretation, bauxite mineralization information extraction and delineation of prospecting target area in the Wuchuan-Zheng'an-Daozhen area; so then, it provides a theory basis for further prospecting.

2. The geology and data sources of study area

2.1 GEOLOGY OF THE STUDY AREA

The research area contains rich bauxite resources located in Wuchuan, Zheng'an and Daozhen County, northern Guizhou, which belongs to Zhengan and Daozhen bauxite belt of the Central Guizhou-southern Chongqing bauxite deposit belt[13-19], such as Wachangping, Xinmin, Sanjiang, Dazuyuan, Xinmu-Yanxi and so on. Beside, the tectonic position of the study area is located in the northern-Guizhou Jurassic Luoshan fold belt of the upper Yangtze block by NNE direction-trending, which developed after the formation of bauxite deposit. Because of NNE-directed compression in this region, the bauxite deposits are strictly controlled by nine synclines, Liyuan syncline, Luchi syncline, Xinmo syncline, Zhang Jiayuan syncline, Huanxi syncline, Taoyuan syncline, Datang syncline, Daozhen syncline and Anchang syncline. Moreover, the ores are all hosted in limbs of the synclines.

The exposed stratigraphic sequence of the study area from oldest to youngest mainly consists of Cambrian, Ordovician, Silurian, Carboniferous, Permian, Triassic,

Dr. Liu Xiao, Geological Survey, China University of Geosciences, Wuhan 430 074, PR China

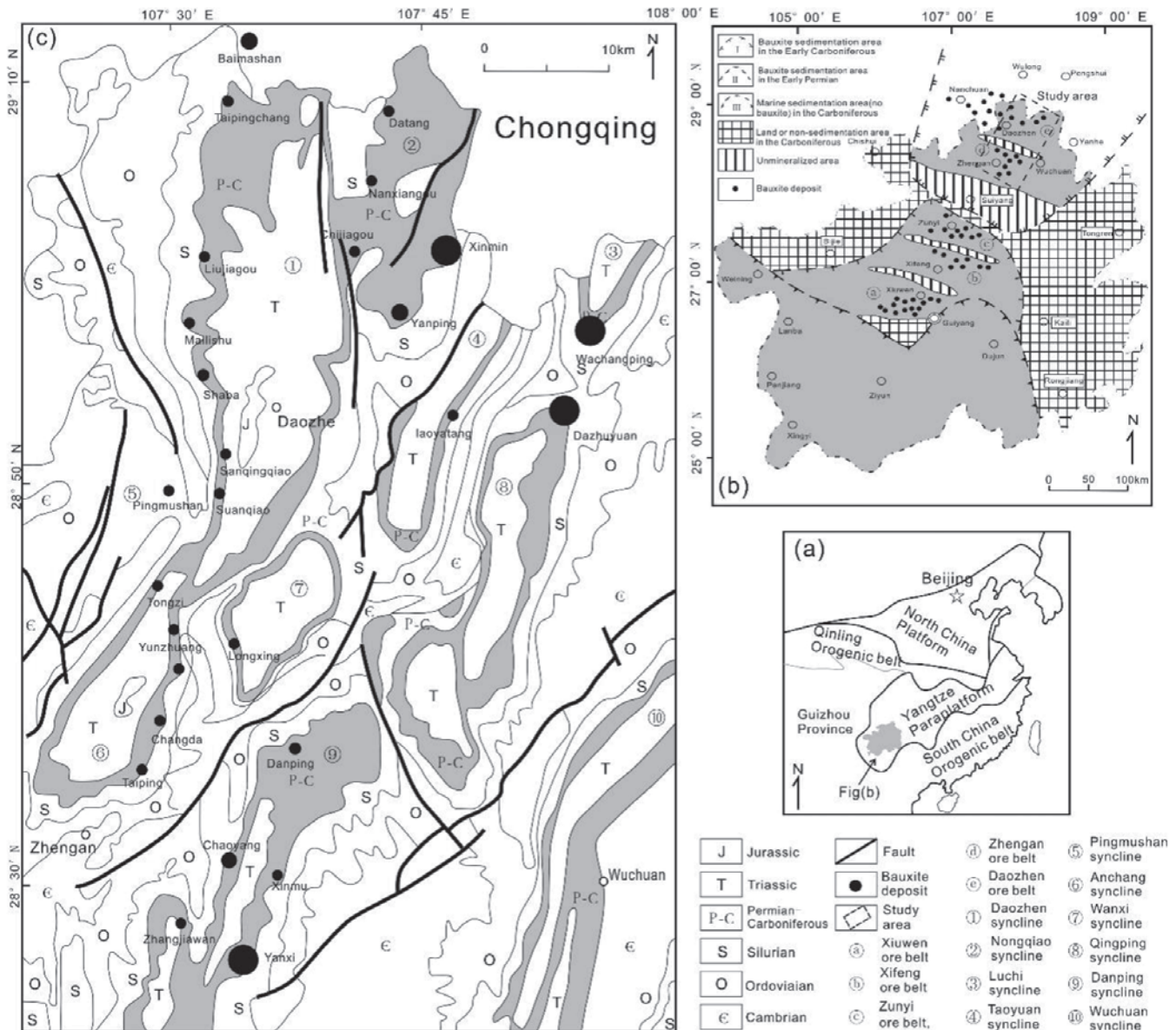


Fig.1 (a) Location map of Guizhou (b) The map showing the location and bauxite deposits of the study area (c) Geological map of the Wuchuan-Zheng'an-Daozhen area (modified from Wu et al., 2008, Liu et al. 2007)

Jurassic and Quaternary units. the Cambrian strata consists of the middle to upper Cambrian dolomite of the Loushanguan Group mainly distributed in the core of anticlines. The Ordovician consists of dolomite, limestone and argillite and the Silurian consists of the lower middle Silurian grayish-green or fuchsia shales, intercalated sandstones and siltstones of Hanjiadian Group. Afterwards, an epirogenic phase caused by a drop of sea level exposed the Hanjiadian Group to intense weathering during upper Silurian to upper carboniferous period. The carboniferous is composed of upper carboniferous limestone of the Huanglong formation, which is mostly eroded and crops out only at a few localities in the region. In the following transgression during the Lower Permian, the seawater submerged the lateritic weathered

materials under warm humid climatic conditions resulting in the formation of the bauxite deposits, which is named Dazhuyuan formation. The coal-rich Triassic units consist of dolomite, limestone, shale and sandstone overlying the bauxite and covered by Jurassic shales and sandstones. Triassic and Jurassic mainly distributed in the core of synclines. the quaternary is sporadically distributed.

The bauxite deposits is overlain by the middle Permian limestone of Qixia formation, Maokou formation and Liangshan formation, and Overlying on the Huanglong formation or the Silurian shale of Hanjiadian formation, respectively. And all of them are parallel unconformity. The bauxite deposits are approximately 2-17m thick, which contains Al_2O_3 of 60%-70%, SiO_2 of 8-15%, and Al/Si is

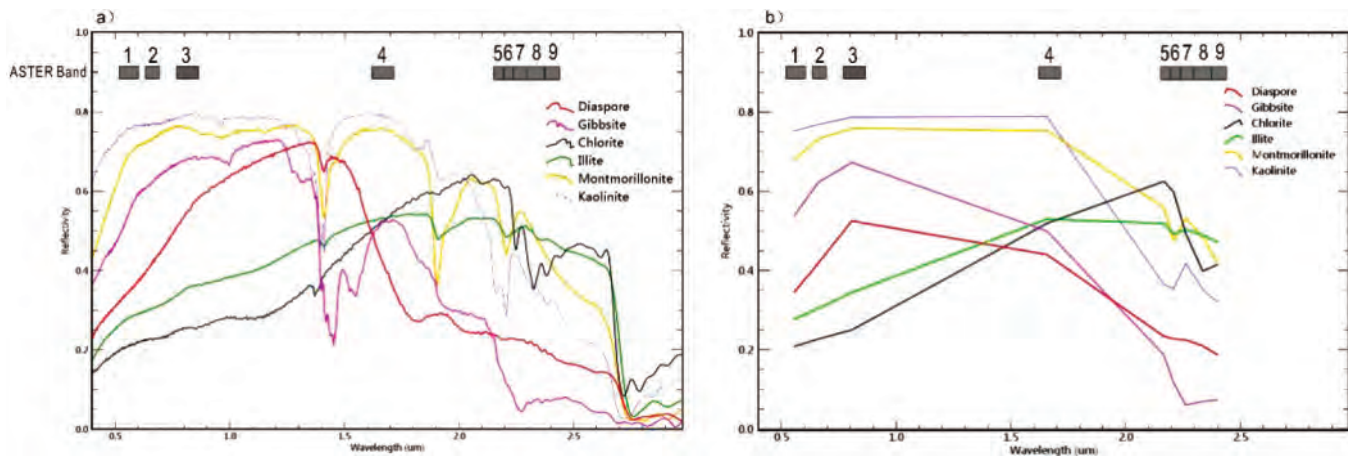


Fig.2 (a) Laboratory reflectance spectra of bauxite deposits; diaspore (red), gibbsite (purple), chlorite (black), illite (green), montmorillonite (orange) and kaolinite (lavender); (b) spectra convolved to ASTER VNIR-SWIR bandpasses

between 4-24. And the main minerals of the ore block are diaspore, kaolinite, chlorite and illite, including a small amount of anatase, zircon, rutile and minute quantity of pyrite, quartz and feldspar[20,21].

2.2 ASTER DATA AND PRE-PROCESSING

Since 2000, ASTER data have been widely and successfully applied to lithological mapping and mineral exploration. The ASTER scenes used in this study were obtained from the NASA EARTH SCIENCE DATA (<https://earthdata.nasa.gov/>) and consist of level 1T for two scenes both acquired in September 29, 2001. The ASTER is the only high spectral resolution multi-spectral scanning system on the first platform on NASA's Earth Observation System AM-1 (EOS AM-1) polar orbiting spacecraft, including three recording channels of visible and near infrared radiation (VNIR) between 0.52 and 0.86 μm , six recording channels of shortwave infrared radiation (SWIR) between 1.6 and 2.43 μm , and five recording channels of thermal infrared radiation (TIR) between 8.125 and 11.65 μm , with 15, 30 and 90 m spatial resolution, respectively. The level 1T data, ASTER level 1 Precision Terrain Corrected Registered At-Sensor Radiance, contains calibrated at-sensor radiance, without atmospheric corrections and corresponds with the ASTER level 1B, that has been geometrically corrected.

Initial pre-processing of the VNIR/SWIR bands of two ASTER datasets involved registering the VNIR and SWIR bands to 15 m pixel size. Those data were converted to surface reflectance by first applying the FLAASH atmospheric correction procedure[22]. Secondly, the two scenes were clipped and combined to form a single image mosaic. Besides, the TIR surface emissivity data were produced from level 1T data using MODTRAN-based atmospheric correction and a temperature-emissivity separation (TES) algorithm developed by Gillespie et al[23]. Mosaicking of the two datasets was achieved by applying a minor adjustment to emissivity values using gains and

offsets calculated the overlap region of the two images.

3. ASTER VNIR+SWIR image analysis

3.1 SPECTRAL REFLECTANCE OF BAUXITE DEPOSITS MINERALS

The reference spectra of the major ore minerals (diaspore, gibbsite) and four gangue minerals (chlorite, illite, montmorillonite and kaolinite) in bauxite deposits (Fig.2) were extracted from the ASTER spectral library (Version 1.2, <http://speclib.jpl.nasa.gov>), and were resampled to the ASTER's VNIR/SWIR bandpasses. Fig.2a shows the laboratory spectra of the seven minerals, and the spectra in Fig.2b are of the six minerals convolved to the ASTER bandpasses. The six minerals show a broad absorption features in 1.39 to 1.41 μm for the OH stretch overtones and 2.16 to 2.20 μm attributed to the combination vibrations of Al-OH and OH stretch[24]. Moreover, the absorption features of ASTER reflectance for diaspore and gibbsite are quite similar and both have a weak reflectance peak at ASTER channel 4.

3.2 ASTER PRINCIPAL COMPONENT ANALYSIS

Principal Component Analysis (PCA) is a very effective mathematical procedure to reduce the dimensionality of data sets and produce uncorrelated output combinations (eigenvector loadings) of variables in such a way that each component successively extracted linear combination and has a smaller variance[25]. A PCA was applied to the original 9-band (VNIR and SWIR) ASTER image of study area to construct nine PCA bands that contain separate information about unique mineral assemblages. Accordingly, the PCA eigenvector loadings and the eigenvalues for the 9-band (VNIR and SWIR) ASTER image are given in Table 1. It shows that the first eigenvalue vector (PC1) to third eigenvalue vector (PC3) contains the almost all percentage of data variance as 74.07%, 20.88% and 3.23%, respectively. The last several PCA components appear noisy as they contain very little variance, much of which is due to noise in the original ASTER data.

TABLE 1: THE PCA EIGENVECTOR OF 9-BAND (VNIR AND SWIR) ASTER IMAGE

Eigen vector	Band 1	Band 2	Band 3	Band 4	Band 5	Band 6	Band 7	Band 8	Band 9	% of variance
PC1	-0.22	-0.31	-0.29	-0.48	-0.33	-0.36	-0.36	-0.32	-0.26	74.07
PC2	0.05	0.17	-0.92	-0.07	0.14	0.13	0.16	0.16	0.15	20.88
PC3	0.51	0.73	0.10	-0.36	-0.11	-0.14	-0.15	-0.10	-0.07	3.23
PC4	-0.11	-0.14	0.21	-0.73	0.07	0.00	0.49	0.25	0.30	0.78
PC5	-0.09	-0.03	0.07	-0.18	0.26	0.26	-0.75	0.19	0.47	0.45
PC6	0.42	-0.34	0.00	-0.20	0.55	0.20	-0.07	0.07	-0.56	0.19
PC7	0.26	-0.17	-0.02	-0.02	0.17	0.16	0.14	-0.82	0.41	0.15
PC8	-0.61	0.41	0.05	-0.15	0.22	0.43	0.05	-0.30	-0.33	0.13
PC9	0.21	-0.15	-0.01	-0.08	-0.64	0.71	-0.01	0.07	-0.08	0.11

3.3 BAUXITE-RELATED LITHOLOGIC INFORMATION EXTRACTION FROM PCA IMAGE

For better discrimination between the main ore-bearing permian-carboniferous stratum, such as the Dazhuyuan group and Liangshan group, and non-mineralization stratum, the three output PCA components (PC1, PC2, and PC3) are selected to constitute false colour composite for distinguishing the ore-bearing stratum (Fig.3). This map shows differences in the distribution of some rock units and contacts between them compared to the published geological map (Fig.2), which support the results obtained from PCA images. The geological interpretations of PCA (PC1, PC2, and PC3) image shows that ore-bearing permian-carboniferous stratum are identified by light red colours. It is easy to depart stratum containing carbonate, such as Cambrian strata, permian-carboniferous strata and part of Triassic strata, from Silurian strata, Ordovician strata and Jurassic strata. This is due to the light red parts containing carbonate or dolomite. Furthermore, the bauxite deposits are located in the light red area, which can narrow reduce the range of the mineral exploration scope.

3.4 MAPPING MINERALIZATION ZONES

PC4 enhances the bauxite mineralization bearing areas as this PC has negative loading of bands 4 and positive loading of band 7. Consequently, the negative part of PC4 indicate the mineralization zone.

To enhance the mineralization information, using median filtering for the image of PC4, and the result image shows as in Fig.4(a).

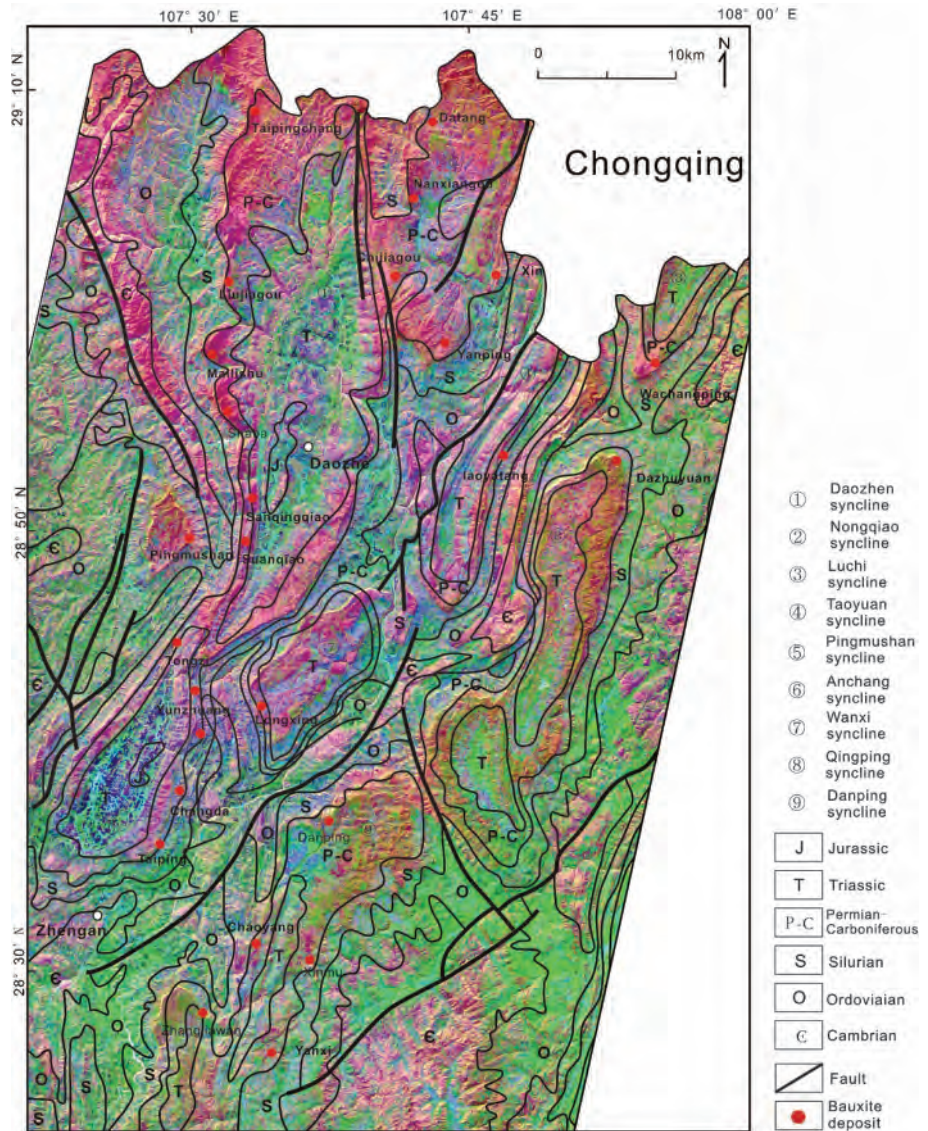


Fig.3 The false colour imaging of ASTER principal component analysis (PC1, PC2, and PC3) RGB image

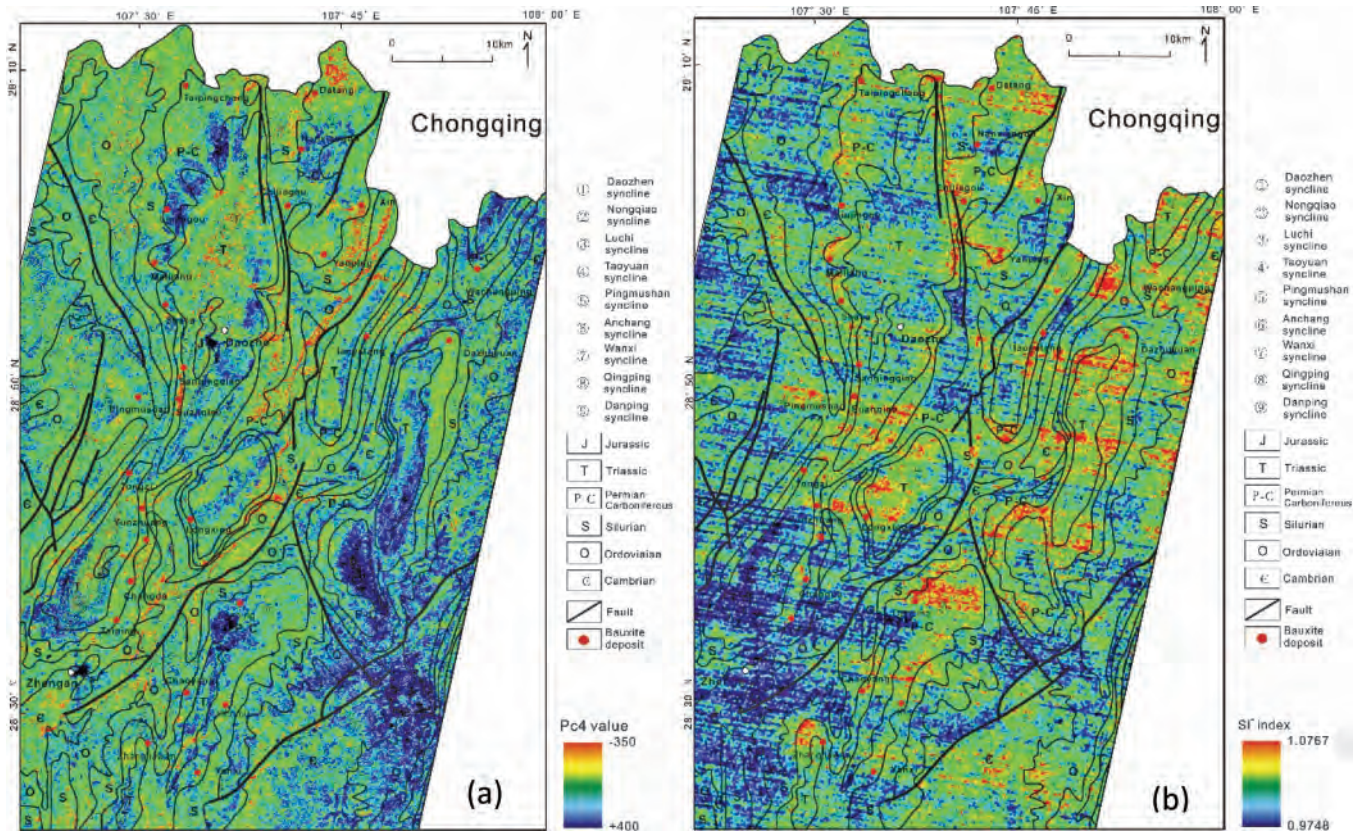


Fig.4 (a) Mineralization zone mapping using PCA transformed indices approach. (b) Image of SI_i^- index of ASTER TIR data

The main ore-bearing stratum, such as the P-C Dazhuyuan group, occurrences negative value of PC4. In addition, major bauxite deposits are located near the negative value area of PC4, which is shown as the yellow-red part in the Fig.4(a).

4. ASTER TIR lithologic indices

Silica, silicate and carbonate rocks occur a strong fundamental spectral feature corresponding to the Si-O and C-O bonds in the thermal atmospheric window region (8-12 μm). ASTER-TIR data have been widely selected for detecting silicates. Based on the middle to far infrared response characteristics of typical rocks [26,27]. Ninomiya et al. proposed several mineralogic indices including the bulk SiO_2 content index (SI) and carbonate index (CI) for detecting mineralogic or chemical composition of silica, carbonate and silicate rocks with ASTER TIR data. SI and CI are defined as $SI = \text{band}_{12} / \text{band}_{13}$ and $CI = \text{band}_{13} / \text{band}_{14}$, respectively. Band_i is surface emissivity data. SI is negative correlation to the bulk SiO_2 content in the silicate rocks and highly sensitive to carbonates. To separated carbonates from bulk SiO_2 content index, SI_i^- is defined as:

$$SI_i^- = \frac{SI}{CI^i} = \frac{\text{band}_{12} + \text{band}_{14}^i}{\text{band}_{13}^{i+1}}$$

However, the noise level is emphasized as IBe grater. For ASTER Level 1B data, $I=3$ is well balanced for the separation

of the carbonate effect and noise level. Cheng Gong used ASTER thermal infrared data to investigate bauxite content of Pingguo bauxite deposit in Guangxi, South China [28].

As the the bauxite ore has a low SiO_2 content, the high value of SI_i^- show the potential mineralization zones of bauxite deposits. To enhance the mineralization information, using median filtering for the image of SI_i^- index, and the result image is shown in Fig.4(b). The image shows that bauxite deposits are located near the high value area of SI_i^- index, which is shown as in the yellow-red part of the Fig. 4(b). Combining the PC4 image (Fig.4.(a)) and the SI_i^- index image (Fig.4(b)), the potential metallogenic area could have been appeared, with consist of lower PC4 data and high SI_i^- value, which provides target area for target area of future bauxite prospecting.

5. Summary and conclusions

Combined with ASTER and existing geological data, this paper used Principal Component Analysis (PCA) and SiO_2 index to produce large-middle scale remote sensing geological interpretation, map the ore-bearing stratum, extract metallogenic zones for bauxite deposits in the Wuchuan-Zheng'an-Daozhen region, northern Guizhou province. The main achievements and understanding are as followings:

- (1) The false colour imaging of ASTER Principal Component Analysis (PC1, PC2, and PC3) could depart ore-bearing

permian-carboniferous stratum containing carbonate from non-mineralization strata, which can narrowly reduce the range of the mineral exploration scope.

- (2) The main ore-bearing stratum, such as P-C Dazhuyuan group, and major bauxite deposits are located near the negative value area of PC4. In addition, bauxite deposits are located near the high value area of SI_i^- index. These are attributed to the reflectance spectra characteristics and low SiO_2 content of bauxite ore.
- (3) Combined the PC4 image containing negative loading of bands 4 and positive loading of band 7 and the SI_i^- index image showing the SiO_2 content of study area, the potential metallogenic area could have been appeared, which consisted of lower PC4 data and high SI_i^- value, which provides target area for target area future bauxite prospecting.

6. References

1. Rowan, L. C., Goetz, A. F. H. and Ashley, R. P. (1977): "Discrimination of hydrothermally altered and unaltered rocks in visible and near-infrared multispectral images." *Geophysics* 42 (3), 522-535.
2. Goetz, A. F. H., Rock, B. N. and Rowan, L. C. (1983): "Remote sensing for exploration: an overview." *Economic Geology* 78 (4), 573-590.
3. Perry, S. L. (2004): Spaceborne and airborne remote sensing systems for mineral exploration-case histories using infrared spectroscopy. In: King, P.L., Ramsey, M.S., Swayze, G.A. (Eds.), *Infrared Spectroscopy in Geochemistry, Exploration Geochemistry, and Remote Sensing*. Mineralogic Association of Canada, London, Canada, pp. 227-240.
4. Henderson, A. F. B., Penfield, G. T. and Grubbs, D. K. (1995): "Satellite Remote Sensing For Aluminum And Nickel Laterites [J]." *Technical Symposium East*, 1984, 481 (6):43-51.
5. Chen, Songling (1990): Remote sensing for study and prospecting of bauxite (gibbsite) in Guangxi [J]. *42(3):83-87*.
6. Babu, P. Suman, Majumdar, T. J. and Bhattacharya, Amit K. (2015): "Study of spectral signatures for exploration of Bauxite ore deposits in Panchpatmali, India [J]." *Geocarto International*, Vol. 30, No. 5, 545-559.
7. Zhang, Wen-long, Hou, Zhao-hua, Li, Ling-jun and Gao, Hai-feng and Yu, Zhan-chao (2015): "Application of SPOT5 data to the remote sensing survey of a bauxite deposit in the Kalimantan area of Indonesia [J]." *Geology and Exploration*, 2015, 51(1): 0157-0164. (in Chinese with English abstract)
8. Yamaguchi, Y., Kahle, A. B., Tsu, H., Kawakami, T. and Pniel, M. (1998): "Overview of advanced spaceborne thermal emission and reflection radiometer (ASTER)." *IEEE Transactions on Geoscience and Remote Sensing* 36(4), 1062-1071.
9. Abrams, M. and Hook, S. (2001): *ASTER Users Handbook (Version 2)*. Jet Propulsion Laboratory, Pasadena, CA, USA.
10. Zhang, Yunfeng, Li, Lingjun and Feng, Chun (2012): The Application of ASTER Data to Bauxite Deposit Pre-survey in Northern China: A Case Study of Mianchi Area, Western Henan. *Remote Sensing for land and Resources*. 1(4)48-52. (in Chinese with English abstract).
11. Cheng, Gong, Zhu, Zhanjun and Gao, Zerun (2012): "Application of ETM+ and ASTER remote sensing data in the prospecting of lateritic bauxite in Laos[]." *Light Metals*, 10. 6-10. (in Chinese with English abstract).
12. Guo, Jiao, Zhu, Guchuang, Zou, Lin, Wang, Ruixue, Han, Ying, Wang, Wei and Xiang, Aiqin (2016): "Remote sensing geological survey of bauxite deposits in Dazhuyuan-Longxing area of northern Guizhou [J]." *Mineral Resources and Geology*, 2016, 30(1):117-121. (in Chinese with English abstract)
13. Wu, G. H., Liu, Y. P. and Zhang, Y. W. (2006): "Geological characters and aluminum ore resources potential in the WuChuan-Zhengan-Daozhen area," *Guizhou. Geology and Prospecting*, 42, 39-43 (in Chinese with English abstract).
14. Han, Zhonghua (2008): "Sedimentary facies characteristics of the Datang bauxite deposit in Daozhen County, Guizhou [J]." *Mineral Resources and Geology*, 22(5). (in Chinese with English abstract).
15. Liu, P. (2007): "Bauxite geology in the Wuchuan-Zhengan-Daozhen area," *Northern Guizhou. Geology and Prospecting* 43, 29-33 (in Chinese with English abstract).
16. Wu, G., Jin, Z., Bao, M. and Mao, Z. (2008): "Bauxite metallogenic regularity in the Wuchuan-Zhengan-Daozhen area," *Northern Guizhou. Geology and Prospecting* 44, 31-35 (in Chinese with English abstract).
17. Jin, Z. G., Wu, G. H., Huang, Z. L., Bao, M. and Zhou, J. X. (2009): "The geochemical characteristics of Wachangping bauxite deposit in Wuchuan County, Guizhou Province, China." *Acta Mineralogica Sinica* 29, 458-462 (in Chinese with English abstract).
18. Yin, X. H. (2009): "Mineralization and metallogenic model for bauxite in the Wuchuan-Zhenan-Daozhen Areas, Northern Guizhou." *Acta Sedimentologica Sinica* 27, 452-457. (in Chinese with English abstract)
19. Liu, X., Wang, Q., Deng, J., Zhang, Q., Sun, S. and Meng, J. (2010a): "Mineralogical and geochemical investigations of the Dajia Salento-type bauxite deposits, western Guangxi, China." *Journal of Geochemical Exploration* 105, 137-152. (in Chinese with English abstract)
20. Gu, Jing, Huang, Zhilong, Fan, Hongpeng, Jin,

- Zhongguo, Yan, Zaifei and Zhang, Jiawei (2016): "Mineralogy, geochemistry, and genesis of lateritic bauxite deposits in the Wuchuan-Zheng'an-Daozhen area, Northern Guizhou Province, China [J]." *Journal of Geochemical Exploration*, 130 (2013) 44-59.
21. Wang, Xiaomei, Jiao, Yangquan and Du, Yuansheng (2013): "REE mobility and Ce anomaly in bauxite deposit of WZD area, Northern Guizhou, China [J]." *Journal of Geochemical Exploration*, 133 (2013) 103-117.
 22. Matthew, M. W., Adler-Golden, S. M., Berk, A. and Felde, G., et al. (2002): "Atmospheric correction of spectral imagery: Evaluation of the FLAASH algorithm with AVIRIS data [J]." *Applied Imagery Pattern Recognition Workshop*, 2002, 5093:157-163.
 23. Gillespie, A., Rokugawa, S. and Matsunaga, T., et al. (2002): "A temperature and emissivity separation algorithm for Advanced Spaceborne Thermal Emission and Reflection Radiometer (ASTER) images [J]." *IEEE Transactions on Geoscience & Remote Sensing*, 2002, 36(4):1113-1126.
 24. Kariuki, P. C. (1999): Analysis of the Effectiveness of Spectrometry in Detecting the Swelling Clay Minerals in Soils M.Sc. thesis International Institute for Aerospace Survey and Earth Sciences, Enschede, The Netherlands 96 pp.
 25. Singh, A. and Harrison, A. (1985): "Standardized principal components." *Int. J. Remote. Sens.* 6, 883-896.
 26. Ninomiya, Y. and Fu, B. (2002): "Quartz index, carbonate index and SiO₂ content index defined for ASTER TIR data [J]." *Journal of Remote Sensing Society of Japan*, 2002, 22:50-60. (in Japanese with English abstract)
 27. Ninomiya, Y., Fu, B. H. and Cudahy, T. J. (2005): "Detecting lithology with Advanced Spaceborne Thermal Emission and Reflection Radiometer (ASTER) multispectral thermal infrared 'radiance-at-sensor' data." *Remote Sens. Environ.* 99, 127-139.
 28. Cheng, Gong, Zeng, Lingyao and Yang, Zhen (2014): "Accumulated bauxite content inversion based on ASTER thermal infrared data." *Light Metals*, 2:5-9. (in Chinese with English abstract)

SEDIMENTARY FEATURES OF THE BAUXITE-BEARING ROCK SERIES IN CENTRAL GUIZHOU

Continued from page 279

delta, diluvial-control depression and diluvial-control lake facies are developed around the paleo-land.

2. The sedimentary facies distribution of ore-bearing rock series in bauxite is jointly controlled by the sedimentary effects of paleogeomorphology, flood and other events in the sedimentary period. Roughly bounded by Yangjiazhuang area, the eastern Xiuwen region shows the sedimentary system of diluvial fan and diluvial uvala, while the western Qingzhen region presents the sedimentary system of diluvial fan, diluvial-control fan delta, and diluvial-control lake.
3. In this region, the diluvial-fan channel has a high sedimentary accumulation rate and a stable thickness distribution. The sheet sand body of diluvial-control delta front is mutually superimposed with underwater gravity flow accretion body. Both are not only the favourable sedimentary places for parent weathering materials, but also the favourable facies belts for bauxite occurrence.
4. The diluvial uvala is obviously affected by the early dissolution, and has strong sedimentary heterogeneity. Especially in areas with strong dissolution at the basement, the bauxitic sediment of large thickness can be formed by filling as the superior sedimentary and metallogenic environment for bauxite deposits, so as to provide a basis for the final formation of industrial ores.

References

1. Chen, Hua and Deng, Chao (2010): "Analys on the Metallogenic Environment of Maochang Bauxite in Guizhou." *Guizhou Geology*, 27(3), pp, 198-201, 2010.
2. Gao, Daode, Sheng, Zhangqi and Shi, Shanhua, et al. (1992): Studies on the Bauxite Deposit in Central Guizhou, China, Guiyang, Gouzhou Science and Technology Press, 1992.
3. Gao, Daode (1996): "A Genetic Model for Sedimentary Type of Bauxite Deposits in central Guizhou." *Guizhou Geology*, 13(2), pp, 166-171, 1996.
4. Liu, Youping, Cheng, Guofan, Zhou, Wenlong and Cui, Tao (2016): "Division of Bauxite mineralization Area (belt) in Guizhou province." *Geological Science and Technology Information*, 35(03), pp. 128-132, 2016.
5. Mo, Jiangping and Li, Jinao (1991): "Metallogenic Environment of Bauxite in central Guizhou." *Geology and Exploration*, (11), pp, 12-18, 1991.
6. Sun, Zhencheng, Cao, Chunchao, Liang, Xinxian and Xu, Kun (1992): "On the Facies Differentiation indicator-Boron and Gallium Content," *Acta Petrolei Sinica*, 13(2), pp, 42-46, 1992.
7. Yang, Ruidong, Yuan, Shiting, Zhang, Xiaodong, Wei, Xiao and Chen, Jiyao (2009): "Mineralization Characteristics and Prospect of Bauxite in West and South of Central Guizhou Lift." *Acta Mineralogica Sinica*, 29(04), pp. 452-457, 2009.
8. Zhang, Baisheng (1984): "Some Problems on the Origin of Carboniferous Bauxite Deposits in central Guizhou." *Geological Review*, 30(6), pp, 553-560, 1984.